

# AN IMPLEMENTATION OF THE GURSON-TVERGAARD-NEEDLEMAN PLASTICITY MODEL FOR ABAQUS STANDARD USING A TRUST REGION METHOD

**D W Beardsmore, M A Wilkes**

Serco Assurance, Birchwood Park, Warrington, Cheshire, WA3 6GA, UK

**A Shterenlikht**

The University of Bristol, Bristol, BS8 1TH, UK

## ABSTRACT

The Gurson-Tvergaard-Needleman (GTN) model is a material plasticity model in which the accumulation of ductile damage is represented by the nucleation, growth and coalescence of micro-voids. The model has been implemented in full for the ABAQUS finite element code. The model supports fully the nucleation, growth, and coalescence of voids, and differs from the porous plasticity model provided in ABAQUS/Standard.

The GTN model is just one model from a particular class of pressure-dependent plasticity models in which the response is dependent on the development of the hydrostatic stress as well as the deviatoric stress tensor. A formal derivation of the constitutive equations is presented in this paper. It is shown that the model can be formally represented by a coupled system of four non-linear equations. A novel approach to solving the equations has been adopted based on a hybrid solution method and a trust region to ensure convergence.

The solution of non-linear equations in more than one variable is usually attempted using iterative methods. For the calculation of a material's response, the method adopted must be sufficiently robust to ensure that the correct result is obtained at each of the material points in the component or structure being modelled. Moreover, the solution method must be as efficient as possible for practical use. In this paper, we present an implementation of a trust region method that allows the solution of the GTN constitutive equations to be derived with confidence.

The method utilises iterative corrections and a trust region surrounding the current estimated solution. In the early stages of the iteration, when the estimate may be far removed from the true solution, the steepest descent method is used to improve the

solution, while at later stages Newton's method, with its superior convergence, is used. A hybrid step (part steepest descent step, part Newton step) may also be taken using Powell's dogleg method with the constraint that the corrections do not take the solution outside the current trust region. A measure of the quality of each step is used to shrink or expand the radius of the trust region during the iteration.

The solution algorithm has been implemented in Fortran 90 as a user subroutine for ABAQUS/Standard. The method provides faster convergence than the porous plasticity model in ABAQUS and allows for the representation of void coalescence. Examples of application of the GTN model to study the response of axisymmetric bars are provided and comparisons are made with the porous plasticity model where appropriate.

## INTRODUCTION

The Gurson-Tvergaard-Needleman (GTN) constitutive model [1-3] is an elastic-plastic model for the representation of ductile materials in Finite Element models. In steels, ductile fracture occurs as a consequence of the nucleation, growth and coalescence of micro-voids. In the model, the micro-voids are represented by a continuous internal variable, the void volume fraction,  $f$ . Ductile fracture is a multi-step process in which a number of micro-mechanical mechanisms occur concurrently: (i) micro-voids are nucleated by decohesion of second-phase inclusions, (ii) micro-voids grow due to plastic straining, (iii) localised diffuse necking occurs as micro-void coalescence begins, and (iv) fracture occurs caused by coalescence of micro-voids and the tearing of the ligaments between them. In the early

stages of ductile fracture, macroscopic diffuse necking is usually observed; in the latter phases the material loses its stress carrying capacity and fracture occurs in macroscopic shear.

In the GTN model, the micro-voids are distributed continuously throughout the material matrix and the void volume fraction is a measure of local material damage. Continuum damage models like the GTN model are necessary for carrying out advanced assessments of engineering structures. Explicit modelling of the micro-voids is not usually practical because of the large difference in the structure and micro-void scales. However, numerical investigations into the effects of arrays of micro-voids have been undertaken and provide valuable insights into the influence of the micro-voids on the material behaviour [4-8]. The evolution of the void volume fraction includes contributions from the nucleation of new micro-voids and the growth of existing micro-voids. The coalescence of micro-voids is represented by including accelerated softening in the expression for the yield surface. An isotropic yield surface is used and the state of yielding depends on the generalised, von Mises stress,  $\sigma_{eq}$ , the hydrostatic stress,  $\sigma_m$ , and the void volume fraction. The GTN model is therefore a pressure-dependent plasticity model.

The model has been implemented as a Fortran 90 subroutine for use with the ABAQUS/Standard Finite Element code. The model has a number of additional features and offers an alternative to the built-in porous plasticity model in ABAQUS/Standard. As well as predicting the void volume fraction, the model calculates the microscopic equivalent plastic strain in the fully dense material, the partitioning of the elastic and plastic strains, and the stress in the material. Integration of the constitutive equations is carried out using the backward Euler method. The incremental forms of the rate equations are non-linear and coupled together, and robust numerical techniques are required to solve them. This paper describes the incremental form of the GTN model equations and the method adopted for their solution. Example calculations are presented to illustrate the use of the model.

## CONSTITUTIVE MODEL

This section describes the GTN constitutive model. The description is divided into three sections providing: (1) a description of the yield function and flow rule, (2) equations for stress and elastic and plastic strain increments, and (3) equations for the evolution of void volume fraction and equivalent plastic strain (the state variables of the model). Later sections will describe how the constitutive equations are solved. Expressions for the consistent Jacobian or linearisation moduli required for implementation of the backward Euler method are provided in the Appendix.

### Yield function and flow rule

The GTN model has the following yield function  $\Phi$  and an identical plastic potential  $g$  [1-3]:

$$g = \Phi = \left( \frac{\sigma_{eq}}{\sigma_0} \right)^2 + 2q_1 f^* \cosh \left( \frac{3q_2 \sigma_m}{2\sigma_0} \right) - (1 + q_2^2 f^{*2}) = 0 \quad (1)$$

where  $\sigma_{eq} = \left( \frac{3}{2} S_{ij} S_{ij} \right)^{1/2}$  is the von Mises equivalent stress,

$\sigma_m = \frac{1}{3} \sigma_{ii}$  is the hydrostatic stress,  $S_{ij} = \sigma_{ij} - \sigma_m \delta_{ij}$  is the

deviatoric stress tensor, and  $\sigma_{ij}$  is the Cauchy stress tensor.<sup>1</sup> The tensor  $\delta_{ij}$  is the Kronecker delta tensor.

The yield function has the following characteristics:

- It reduces to the von Mises yield function when  $f^* = 0$ .
- It varies linearly with  $f^*$  for  $\sigma_m = 0$ , as in pure shear.
- It depends on stress tri-axiality,  $\sigma_m/\sigma_0$ , through a hyperbolic function, as suggested by Rice and Tracey [9].

Equation (1) was originally suggested by Gurson who carried out a limit analysis of a spherical cavity in a rigid plastic medium [1]. The constants  $q_1$ ,  $q_2$  were introduced by Tvergaard to obtain better agreement with his study of localised shear band bifurcations using a periodic array of voids [2, 3]. Koplik and Needleman [4] found that the best predictions of growth and coalescence were obtained with  $q_1 = 1.25$  and  $q_2 = 1$ .

The yield stress  $\sigma_0$  represents the radius of the yield surface and is assumed to be some function of the microscopic equivalent plastic strain in the undamaged material,  $\sigma_0 = \sigma_0(\epsilon_{eqM}^p)$ . The Fortran 90 code allows the use of several functional forms for  $\sigma_0$  including power-law, modified Ramberg-Osgood, and look-up table forms.

When  $f^*$  is non-zero the hydrostatic stress effects the plastic flow as illustrated in Fig. 1. The solid curves are for Gurson's original model with  $q_1 = q_2 = 1$ . The broken curve is the curve for  $f^* = 0.1$  using Koplik and Needleman's suggested constants.

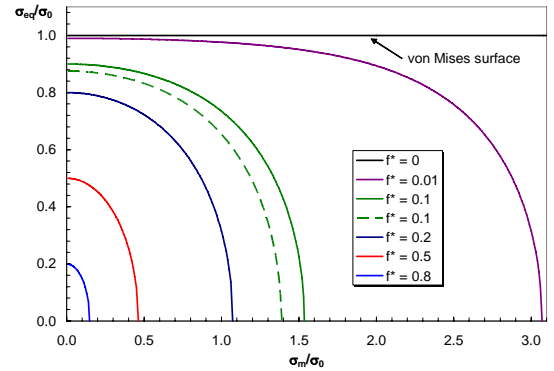


Fig. 1. Effect of hydrostatic stress on plastic flow for different values of  $f^*$

In Gurson's original model,  $f^* = f$ . A further modification by Tvergaard and Needleman [10] made  $f^*$  a bilinear function of  $f$  to account for the rapid coalescence of micro-voids at fracture. At low values of void volume fraction,  $f^* = f$ , but above some critical void volume fraction  $f_c$  the value of  $f^*$  increases more rapidly to give increased softening as the micro-voids coalesce. In our implementation of  $f^*$  a plateau is added above the void volume fraction  $f_f$  at which fracture occurs:

<sup>1</sup> Indicinal, tensor notation will be used consistently throughout this paper.

$$f^* = \begin{cases} f & f \leq f_c \\ f_c + \left( \frac{f_u^* - f_c}{f_f - f_c} \right) (f - f_c) & f_c < f < f_f \\ f_u^* & f \geq f_f \end{cases} \quad (2)$$

Values of  $f_c = 0.15$  and  $f_f = 0.25$  are suggested in Reference [10]. The constant  $f_u^*$  is the value of  $f^*$  at zero stress so that as  $f \rightarrow f_f$ ,  $f^* \rightarrow f_u^*$  and the material loses the ability to transmit stress. The plateau in Eq. (2) is required to ensure that the stress remains at zero once fracture has occurred. Setting  $\sigma_{eq} = \sigma_m = 0$  gives  $f_u^* = 1/q_1$ . The constants must be such that  $f_u^* > f_f$  for accelerated softening to occur.

Figure 2 shows the effect of coalescence on the plastic flow for five different values of hydrostatic stresses. These curves are plotted using  $q_1 = q_2 = 1$  and  $f_c = 0.15$  and  $f_f = 0.25$ . A rapid decrease in  $\sigma_{eq}$  occurs when the void volume fraction is above  $f_c$ . There is no coalescence effect, however, if the hydrostatic stress exceeds  $\frac{\sigma_m}{\sigma_0} = -\frac{2}{3q_2} \ln(q_1 f_c)$  or about 1.265 in this case.

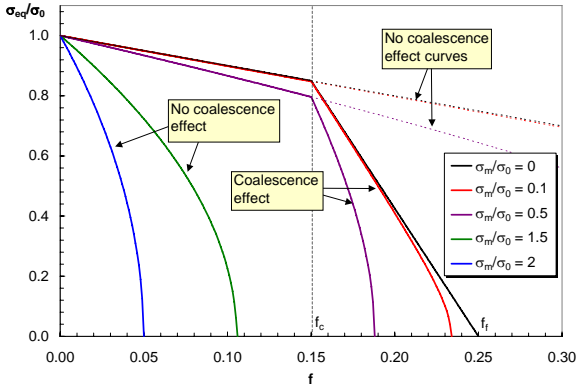


**Fig. 2. Effect of coalescence on plastic flow for different values of hydrostatic stress**

The flow rule or normality rule for the plastic strain rate, by the application of the chain rule to Eq. (1), is:

$$\Delta \varepsilon_{ij}^p = \Delta \Lambda \frac{\partial g}{\partial \sigma_{ij}} = \Delta \Lambda \left( \frac{\partial g}{\partial \sigma_{eq}} \frac{\partial \sigma_{eq}}{\partial \sigma_{ij}} + \frac{\partial g}{\partial \sigma_m} \frac{\partial \sigma_m}{\partial \sigma_{ij}} \right) \quad (3)$$

where  $\Delta \Lambda$  is a positive scalar as the plastic deformation must be irreversible [11]. This is the incremental form of the rate equation: all rate equations in this paper will be written in incremental form as this is more convenient for our purposes. The flow rule may be written in terms of the deviatoric and hydrostatic plastic strain increments,

$$\Delta \varepsilon_{ij}^p = \Delta \varepsilon_{ij}^d + \Delta \varepsilon_m^p \delta_{ij} \quad (4)$$

where the increases in the deviatoric plastic strain tensor  $\Delta \varepsilon_{ij}^d$  and the hydrostatic plastic strain  $\Delta \varepsilon_m^p$  are given by:

$$\Delta \varepsilon_{ij}^d = \Delta \Lambda \frac{\partial g}{\partial \sigma_{eq}} n_{ij} \quad (5a)$$

$$\Delta \varepsilon_m^p = \frac{1}{3} \Delta \Lambda \frac{\partial g}{\partial \sigma_m} \quad (5b)$$

with  $n_{ij} = \frac{\partial \sigma_{eq}}{\partial \sigma_{ij}} = \frac{3}{2} \frac{S_{ij}}{\sigma_{eq}}$  and  $\frac{\partial \sigma_m}{\partial \sigma_{ij}} = \frac{1}{3} \delta_{ij}$ . Using the usual definition of the equivalent plastic strain rate [11], the increment in equivalent plastic strain is:

$$\Delta \varepsilon_{eq}^p = \sqrt{\frac{2}{3}} \Delta \varepsilon_{ij}^d = \Delta \Lambda \frac{\partial g}{\partial \sigma_{eq}} \quad (5c)$$

Eq. (5a) can therefore be written in the alternative form:

$$\Delta \varepsilon_{ij}^d = \Delta \varepsilon_{eq}^p n_{ij} \quad (5d)$$

Eliminating the scalar  $\Delta \Lambda$  from Eqs. (5b) and (5c) results in the consistency condition:

$$\Delta \varepsilon_{eq}^p \frac{\partial g}{\partial \sigma_m} = 3 \Delta \varepsilon_m^p \frac{\partial g}{\partial \sigma_{eq}}. \quad (6)$$

### Calculation of stress and elastic and plastic strain increments

In a finite element calculation, the increment in the total strain tensor is passed to the constitutive model, which must calculate the stress and elastic and plastic strain increments. The total strain increment tensor  $\Delta \varepsilon_{ij}$  can be considered as the sum of the plastic strain tensor  $\Delta \varepsilon_{ij}^p$  and the elastic strain tensor  $\Delta \varepsilon_{ij}^e$  increments.

$$\Delta \varepsilon_{ij} = \Delta \varepsilon_{ij}^e + \Delta \varepsilon_{ij}^p \quad (7)$$

The Cauchy stress at the end of an increment can be calculated by adding the product of the fourth-order elasticity tensor and elastic strain increment tensor to the stress at the start of the increment,

$$\sigma_{ij} = \sigma_{ij}^0 + E_{ijkl} \Delta \varepsilon_{kl}^e \quad (8)$$

where, for isotropic elasticity, the elasticity tensor is determined by Hooke's law:

$$E_{ijkl} = 2G \delta_{ik} \delta_{jl} + \lambda \delta_{ij} \delta_{kl} \quad (9)$$

where  $G$  and  $\lambda$  are Lamé's constants, related to Young's modulus  $E$  and Poisson's ratio  $\nu \leq 1/2$  according to  $G = E/(2(1+\nu))$ ,  $K = E/(3(1-2\nu))$ , and  $\lambda = K - (2/3)G$ .

If an initial assumption is made that all of the strain increment  $\Delta \varepsilon_{ij}$  is elastic, an elastic prediction of the stress tensor at the end of the increment can be calculated using

$$\sigma_{ij}^e = \sigma_{ij}^0 + E_{ijkl} \Delta \varepsilon_{kl}. \quad (10)$$

This prediction will be correct if it gives a negative value for the yield function,  $\Phi < 0$  using Eq. (1). This indicates that the material is behaving elastically, which occurs when the material point is below the yield surface or moves off the yield surface due

to unloading. In such cases, the stress tensor is the elastic-predictor stress tensor and the elastic strain increment tensor is the total strain increment tensor. Otherwise, the stress tensor must be obtained by subtracting the effect of the plastic strains from the elastic prediction. As the tensors  $n_{ij}$  and  $\delta_{ij}$  are orthogonal,  $n_{ij}\delta_{ij} = 0$ , this operation results in orthogonal correction terms for the case of isotropic elasticity:

$$\sigma_{ij} = \sigma_{ij}^e - E_{ijkl}\Delta\epsilon_{kl}^p = \sigma_{ij}^e - 2G\Delta\epsilon_{eq}^p n_{ij} - 3K\Delta\epsilon_m^p \delta_{ij}, \quad (11)$$

Figure 3 shows the construction of the new stress tensor  $\sigma_{ij}$  on the new yield surface from the old value  $\sigma_{ij}^0$  on the initial yield surface.

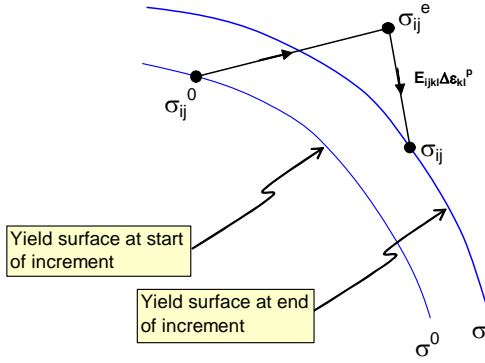


Fig. 3 construction of new stress tensor during yielding

The stress tensor can be separated into deviatoric and hydrostatic components:

$$\sigma_{ij} = S_{ij} + \sigma_m \delta_{ij} = \frac{2}{3} \sigma_{eq} n_{ij} + \sigma_m \delta_{ij} \quad (12)$$

and for consistency with Eq. (11),

$$S_{ij} = S_{ij}^e - 2G\Delta\epsilon_{eq}^p n_{ij} \quad (13a)$$

$$\sigma_m = \sigma_m^e - 3K\Delta\epsilon_m^p \quad (13b)$$

where  $S_{ij}^e$  is the elastic-predictor deviatoric stress tensor corresponding to  $\sigma_{ij}^e$ . Eq. (13a) shows that the correction represents a return to the yield surface in deviatoric stress space in the negative direction of the vector  $n_{ij}$ . This observation means that  $n_{ij}$ , the deviatoric stress tensor  $S_{ij}$ , and the elastic-predictor deviatoric stress tensor  $S_{ij}^e$  must be co-axial with each other.

Defining the elastic-predictor von Mises stress as  $\sigma_{eq}^e = \left( \frac{3}{2} S_{ij}^e S_{ij}^e \right)^{1/2}$  allows  $n_{ij}$  to be calculated from the elastic-predictor quantities,

$$n_{ij} = \frac{3}{2} \frac{S_{ij}^e}{\sigma_{eq}^e} = \frac{3}{2} \frac{S_{ij}^e}{\sigma_{eq}^e} \quad (14)$$

and Eq. (13a) can be written in equivalent stress form:

$$\sigma_{eq} = \sigma_{eq}^e - 3G\Delta\epsilon_{eq}^p. \quad (15)$$

### Equivalent plastic strain and void volume fraction

The void volume fraction  $f$  represents the number and size of micro-voids in the material. This is one of the state variables in the model. The other state variable is the equivalent plastic strain in the fully dense, undamaged material,  $\epsilon_{eqM}^p$ . This is a microscopic internal property and should not be confused with  $\epsilon_{eq}^p$ , which is a macroscopic property representing the equivalent plastic strain in the damaged material.

The principle of equivalent work may be used to calculate the increment of the equivalent plastic strain in the fully dense material,  $\Delta\epsilon_{eqM}^p$ . The increment of plastic work per unit volume is [11]:

$$dW_p = \sigma_{ij} \Delta\epsilon_{ij}^p = (1-f) \sigma_0 \Delta\epsilon_{eqM}^p \quad (16)$$

so, using Eq. (4) to substitute for  $\Delta\epsilon_{ij}^p$  and Eq. (12) to substitute for  $\sigma_{ij}$  on the left-hand side,

$$\Delta\epsilon_{eqM}^p = \frac{\sigma_{eq} \Delta\epsilon_{eq}^p + 3\sigma_m \Delta\epsilon_m^p}{\sigma_0 (1-f)}. \quad (17)$$

The evolution of micro-voids in the material can be considered to be the sum of terms representing the nucleation of new micro-voids and the growth of existing micro-voids:

$$\Delta f = \Delta f_{nuc} + \Delta f_{gr} \quad (18)$$

The nucleation of new micro-voids depends on the plastic strain in the material. The rate at which new micro-voids nucleate is proportional to the equivalent plastic strain rate in the fully dense material. This can be written

$$\Delta f_{nuc} = A \Delta\epsilon_{eqM}^p \quad (19)$$

where  $A$  is a constant that is chosen so that the strain required for nucleation follows a normal distribution with mean  $\epsilon_N$  and standard deviation  $s_N$ :

$$A = \frac{f_N}{s_N \sqrt{2\pi}} \exp \left\{ -\frac{1}{2} \left( \frac{\epsilon_{eqM}^p - \epsilon_N}{s_N} \right)^2 \right\}. \quad (20)$$

In Eq. (20),  $f_N$  represents the void volume fraction due to nucleating particles.

The growth of existing voids is governed by the requirement that the volume of the material matrix is constant during plastic straining:

$$\Delta f_{gr} = (1-f) \Delta\epsilon_{ii}^p = 3(1-f) \Delta\epsilon_m^p. \quad (21)$$

The total increase in the void volume fraction due to nucleation and growth of micro-voids is therefore, by adding Eq. (19) and Eq. (21):

$$\Delta f = A \Delta\epsilon_{eqM}^p + 3(1-f) \Delta\epsilon_m^p. \quad (22)$$

## SOLUTION OF GTN CONSTITUTIVE EQUATIONS

The state of stress and strain and the ductile damage can be calculated if the values of the scalars  $\Delta\mathcal{E}_{eq}^p$ ,  $\Delta\mathcal{E}_m^p$ ,  $\sigma_{eq}$ ,  $\sigma_m$ ,  $\Delta f$  and  $\Delta\mathcal{E}_{eqM}^p$  can be determined. These six scalars may be obtained as the solution of Eqs. (1), (6), (13b), (15), (17), and (22). Once the equations have been solved, the stress and strain tensors can be obtained simply:

- The stress tensor can be calculated from Eq. (11) or (12).
- The increment in the plastic strain tensor  $\Delta\mathcal{E}_{ij}^p$  can be calculated using Eqs. (4) and (5d).
- The increment in the elastic strain tensor  $\Delta\mathcal{E}_{ij}^e$  can be obtained by Eq. (7).

### Simplification and re-arrangement of equations

The number of equations can be reduced to four, simplifying the problem, by using Eqs. (13b) and (15) to substitute for and eliminate  $\sigma_m$  and  $\sigma_{eq}$  from the other equations. In this paper, this substitution is done implicitly: that is, we retain the terms  $\sigma_m$  and  $\sigma_{eq}$  in all expressions on the understanding that Eqs. (13b) and (15) can be used to eliminate them. Computationally, implicit substitution corresponds to the use of intermediate variables to represent the von Mises and hydrostatic stresses.

The four key equations that must be solved can now be collected together. For convenience the equations are re-written in the standard form  $\mathbf{f} = \mathbf{0}$  where  $\mathbf{f}$  is a vector of functions.

$$f_1 = \Delta\mathcal{E}_{eq}^p \frac{\partial g}{\partial \sigma_m} - 3\Delta\mathcal{E}_m^p \frac{\partial g}{\partial \sigma_{eq}} = 0 \quad (23a)$$

$$f_2 = \left( \frac{\sigma_{eq}}{\sigma_0} \right)^2 + 2q_1 f^* \cosh\left( \frac{3q_2 \sigma_m}{2\sigma_0} \right) - (1 + q_2^2 f^{*2}) = 0 \quad (23b)$$

$$f_3 = \Delta\mathcal{E}_{eqM}^p - \frac{\sigma_{eq} \Delta\mathcal{E}_{eq}^p + 3\sigma_m \Delta\mathcal{E}_m^p}{\sigma_0(1-f)} = 0 \quad (23c)$$

$$f_4 = \Delta f - A\Delta\mathcal{E}_{eqM}^p - 3(1-f)\Delta\mathcal{E}_m^p = 0 \quad (23d)$$

These equations are of the form developed by Aravas for a general class of pressure-dependent plasticity models [12]. Aravas suggests solving the first two equations for  $\Delta\mathcal{E}_{eq}^p$ ,  $\Delta\mathcal{E}_m^p$  (and  $\sigma_{eq}$ ,  $\sigma_m$  by implicit substitution). Newton's method is suggested for solving the two equations. As values of the state variables  $\Delta f$  and  $\Delta\mathcal{E}_{eqM}^p$  are required for each iteration of Newton's method, Aravas suggests these be obtained by solving Eqs. (23c) and (23d) as a separate nested, sub-problem, again by making use of Newton's method. There are a number of difficulties with Aravas's method:

- Newton's method may not converge, or may converge to an incorrect solution.
- The use of nested applications of Newton's method means that many iterations are required to obtain a solution. Experimentation with the procedure shows that 10-20 iterations are typically required to solve the main problem, Eqs. (23a) and (23b), each requiring 10-

20 iterations to solve the sub-problem, Eqs. (23c) and (24d). Thus, up to 400 iterations on the sub-problem might be required.

- Newton's method requires partial derivatives of the functions with respect to each of the unknown variables. For the main problem, these expressions must take into account the coupling with the state variables in the sub-problem. The equations for doing this are provided by Aravas but require that a particular  $2 \times 2$  matrix be non-singular and inverted at each iteration step.
- For some values of  $\Delta\mathcal{E}_{eq}^p$ ,  $\Delta\mathcal{E}_m^p$  that are selected as trial values by Newton's method, the sub-problem might have no solution.

These problems mean that small increments must be taken to ensure a correct solution is achieved.

### Solution by a trust region method

In this section an iterative method for solving the four equations as one set is described. The method makes use of Newton's method in the latter stages of the iteration, when the estimate of the solution is close to the true solution, but uses a more cautious approach for the initial iterations. For convenience, the unknown quantities are collected into a vector  $\mathbf{x}$ :

$$\mathbf{x} = \left( \Delta\mathcal{E}_m^p, \Delta\mathcal{E}_{eq}^p, \Delta f, \Delta\mathcal{E}_{eqM}^p \right)^T \quad (24)$$

Given an approximation to  $\mathbf{x}_n$ , Newton's method gives a new approximation by adding a correction step  $\mathbf{h}$  obtained by solving a linear system:

$$\mathbf{J}(\mathbf{x}_n)\mathbf{h} = -\mathbf{f}(\mathbf{x}_n) \quad (25a)$$

$$\mathbf{x}_{n+1} = \mathbf{x}_n + \mathbf{h} \quad (25b)$$

Successive iteration on Eqs. (25) is used to obtain a solution to the desired accuracy. However, depending on the nature of  $\mathbf{f}$  the iteration may fail to converge or converge on the wrong solution, especially if the initial approximation for  $\mathbf{x}$  is far removed from the true solution.

The matrix  $\mathbf{J}$  is the Jacobian, calculated from the partial derivatives of the functions with respect to each of the unknown variables:

$$(\mathbf{J})_{ij} = \left\{ \frac{\partial f_i}{\partial x_j} \right\} \quad (26)$$

The solution of Eqs. (23) is also the global minimiser for the sum of squares of the function values,  $F(\mathbf{x})$ :

$$F(\mathbf{x}) = \frac{1}{2} \|f(\mathbf{x})\|^2 = \frac{1}{2} \sum_{i=1}^4 f_i(\mathbf{x})^2 \quad (27)$$

Hence, instead of solving Eqn. (25a), a correction  $\mathbf{h}$  can be obtained by minimising the sum of squares of  $\mathbf{J}(\mathbf{x})\mathbf{h} + \mathbf{f}(\mathbf{x})$ , or

$$L(\mathbf{h}) = F(\mathbf{x}) + \mathbf{f}(\mathbf{x})^T \mathbf{J}(\mathbf{x})\mathbf{h} + \frac{1}{2} \mathbf{h}^T \mathbf{J}(\mathbf{x})^T \mathbf{J}(\mathbf{x})\mathbf{h} \quad (28)$$

The value of  $\mathbf{h}$  which minimises Eq. (28) can be obtained using

the method of steepest descent. The direction in which  $F(\mathbf{x})$  decreases most rapidly is calculated using:

$$\mathbf{h}_{sd} = -\nabla F(\mathbf{x}) = -\mathbf{J}(\mathbf{x})^T \mathbf{f}(\mathbf{x}) \quad (29)$$

The step size which minimises Eq. (28) is of the form  $\alpha \mathbf{h}_{sd}$  where  $\alpha$  is a scalar. Substituting  $\mathbf{h} = \alpha \mathbf{h}_{sd}$  in Eq. (28) gives:

$$L(\alpha \mathbf{h}_{sd}) = F(\mathbf{x}) + \alpha \mathbf{h}_{sd}^T \mathbf{J}(\mathbf{x})^T \mathbf{f}(\mathbf{x}) + \frac{1}{2} \alpha^2 \mathbf{h}_{sd}^T \mathbf{J}(\mathbf{x})^T \mathbf{J}(\mathbf{x}) \mathbf{h}_{sd} \quad (30)$$

Setting  $\partial L / \partial \alpha = 0$  leads to

$$\alpha = \frac{\|\mathbf{h}_{sd}\|}{\|\mathbf{J}(\mathbf{x}) \mathbf{h}_{sd}\|} \quad (31)$$

The solution method we have adopted uses the steepest descent direction in the initial stages of the iteration, and switches to Newton's method in the final stages. At each iteration, the correction  $\mathbf{h}$  is constrained to lie within a 4-dimensional trust region or 'ball' in the space of  $\mathbf{x}$  of radius  $\Delta$ . At intermediate iterations, a hybrid step, consisting of part steepest descent step and part Newton step, is calculated using Powell's dogleg method. The correction  $\mathbf{h}_{dl}$  is determined as follows:

- If Newton's step lies inside the trust region, this is used,  $\mathbf{h}_{dl} = \mathbf{h}_n$ .
- If the steepest descent step  $\alpha \mathbf{h}_{sd}$  lies inside the trust region but Newton's step  $\mathbf{h}_n$  lies outside, a hybrid step is taken to the boundary of the trust region (see below).
- If both the steepest descent step  $\alpha \mathbf{h}_{sd}$  and Newton's step  $\mathbf{h}_n$  lie outside the trust region, the steepest descent is used, but is scaled to the boundary of the trust region,  $\mathbf{h}_{dl} = (\Delta / \|\mathbf{h}_{sd}\|) \mathbf{h}_{sd}$ .

The algorithm is shown in Fig. 4.

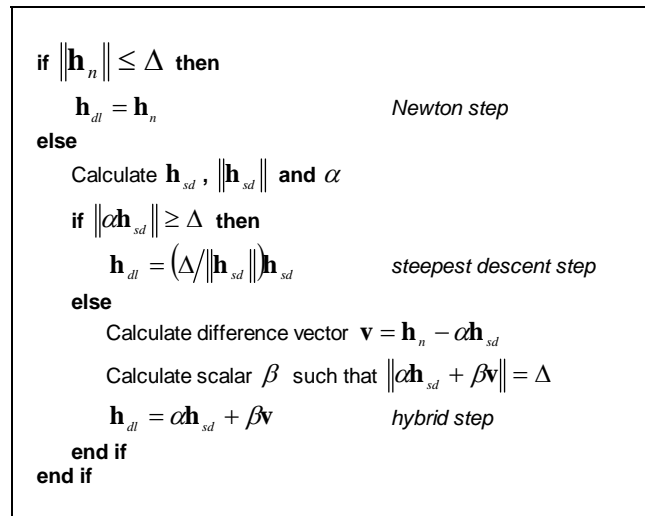


Fig. 4. Algorithm for determining constrained hybrid step  $\mathbf{h}_{dl}$

In each case, the step is not allowed to go outside the trust region,

$$\|\mathbf{h}_{dl}\| \leq \Delta.$$

Powell's dogleg algorithm is used to determine the hybrid steps. A typical hybrid step is illustrated in Fig. 5. The value of  $\beta$  in Fig. 4 is the fraction of the difference  $\mathbf{h}_n - \alpha \mathbf{h}_{sd}$  that must be added to  $\alpha \mathbf{h}_{sd}$  to give a step to the boundary. This can be obtained by setting the length of the step to  $\Delta$  and taking the positive solution of the resulting quadratic equation.

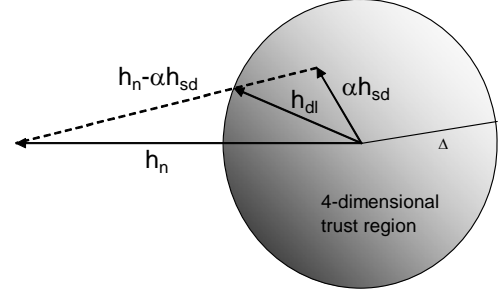


Fig. 5 Illustration of a dogleg correction step

Once the correction step  $\mathbf{h}_{dl}$  has been determined, a gain ratio  $\rho$  is calculated, which is the ratio of the actual decrease in  $F(\mathbf{x})$  to the predicted decrease, and measures the quality of the step:

$$\rho = \frac{F(\mathbf{x}) - F(\mathbf{x} + \mathbf{h}_{dl})}{L(\mathbf{0}) - L(\mathbf{h}_{dl})} \quad (32)$$

When  $\rho$  is positive, the step is good and a new estimate of the solution vector is calculated using Eq. (25b). In this case, the trust region is expanded by a factor that depends on  $\rho$ . When  $\rho$  is zero or negative, the step is rejected, the radius of the trust region is reduced, and a new step is determined by a repeated application of the algorithm in Fig. 4.

Figure 6 shows the algorithm used to control the radius of the trust region.

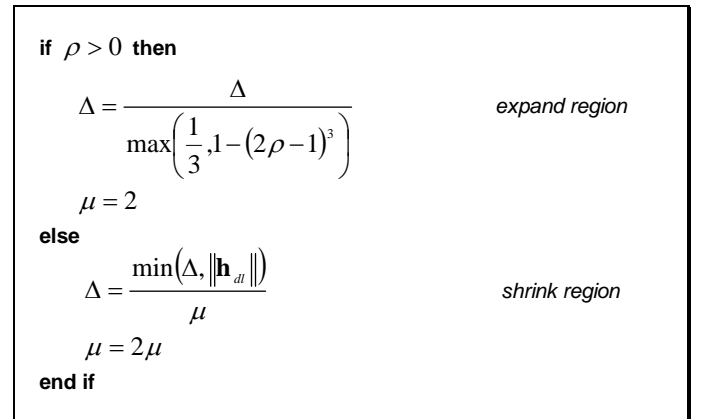


Fig. 6. Algorithm for changing radius of trust region

The trust region shrinks and expands during the iteration as it adapts to the quality of each step. The iteration can be stopped when the solution has been found to sufficient accuracy or when the trust region is very small.

## EXAMPLE CALCULATIONS

Some example calculations illustrating the use of the model are presented in this section. To provide a comparison of the results with the porous plasticity model in ABAQUS/Standard the

coalescence effect was turned off by setting  $f_c = 1$  and  $f_f = 2$  so that  $f^* = f$ .

The first calculation considers a single volume element in hydrostatic tension, with an equal displacement applied to each of the three orthogonal directions. The volume element, boundary conditions and applied displacement constraints are shown in Fig. 7.

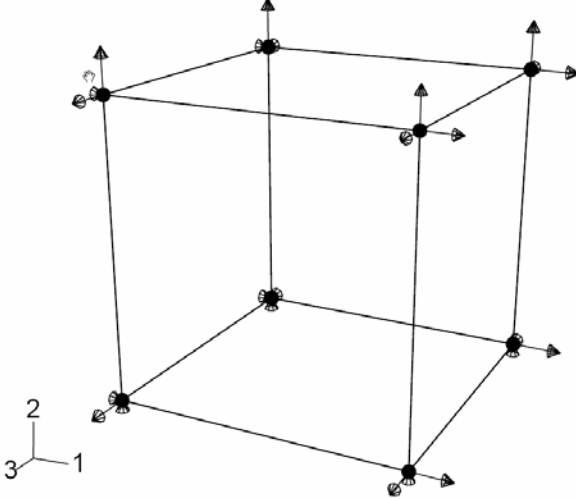


Fig. 7. Single 3D element in hydrostatic tension

The material properties were taken from Aravas's paper [12]. A power-law representation for  $\sigma_0(\varepsilon_{eqM}^p)$  was used of the form:

$$\frac{\sigma_0}{\sigma_{PL}} = \left( \frac{\sigma_0}{\sigma_{PL}} + \frac{3G}{\sigma_{PL}} \varepsilon_{eqM}^p \right)^N \quad (33)$$

with  $E = 2GPa$ ,  $\nu = 0.3$ ,  $\sigma_{PL} = 667MPa$ , and  $N = 0.1$ . Nucleation of voids was defined with  $f_N = 0.04$ ,  $\varepsilon_N = 0.3$ ,  $s_N = 0.1$ . The Tvergaard constants in the yield function were  $q_1 = 1.5$ ,  $q_2 = 1$ . An initial void volume fraction of 0.04 was assumed.

Figures 8 and 9 show results for  $\sigma_m/\sigma_{PL}$  and void volume fraction respectively as a function of the volumetric strain  $\varepsilon_{ii}$ . Excellent agreement was obtained with the results of Aravas [12] and with the use of the ABAQUS/Standard porous plasticity model.

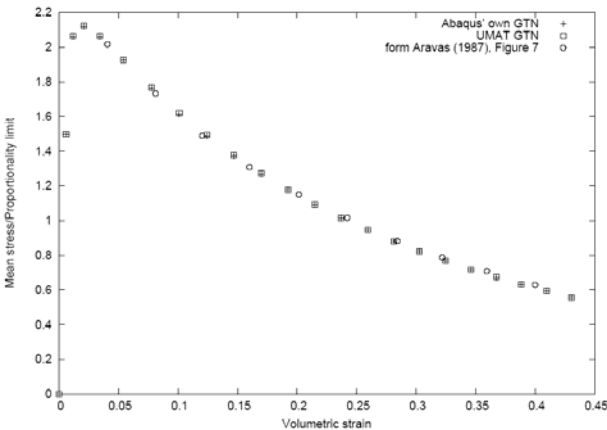


Fig. 8. Plot of  $\sigma_m/\sigma_{PL}$  against volumetric strain  $\varepsilon_{ii}$ .

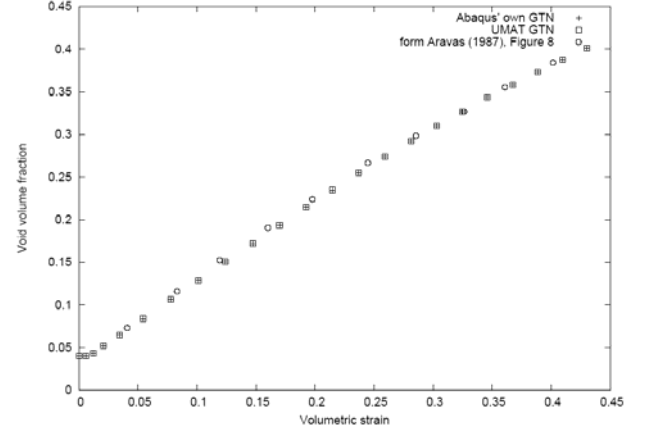


Fig. 9. Plot of  $f$  against volumetric strain  $\varepsilon_{ii}$ .

The second calculation presented is an analysis of an axisymmetric bar in tension. Fig. 10 shows the mesh. Only one half of the bar was modelled due to symmetry, the length of the half-bar was  $l_w = 26mm$ . The radius of the bar was  $r_w = 3mm$ .

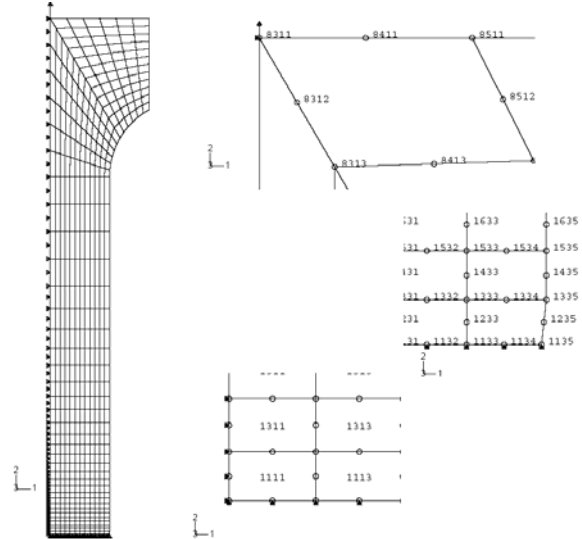


Fig. 10. Finite element model of round bar

A neck was introduced at the mid-plane by moving node 1135 inwards to a radius of  $r_a = 2.995mm$ . A displacement was applied to node 8311 at the top of the model (nodes 8411, 8511, etc running along the top of the model were constrained to displace vertically with node 8311.)

For the material model,  $E = 2.1GPa$ ,  $\nu = 0.3$ ,  $\sigma_{PL} = 468MPa$ , and a look-up table was used to prescribe  $\sigma_0(\varepsilon_{eqM}^p)$ . Void nucleation was turned off using  $f_N = 0.0$ ,  $\varepsilon_N = 0.0$ ,  $s_N = 0.1$ . The Tvergaard constants in the yield function were  $q_1 = 1.5$ ,  $q_2 = 1$ . An initial void volume fraction of 0.002 was assumed.

Figures 11 and 12 show the load applied to the top of the bar as a function of the average axial strain and the contraction at the symmetry plane respectively. The load in each case has been normalised with respect to the elastic limit stress and the cross-sectional area of the specimen.

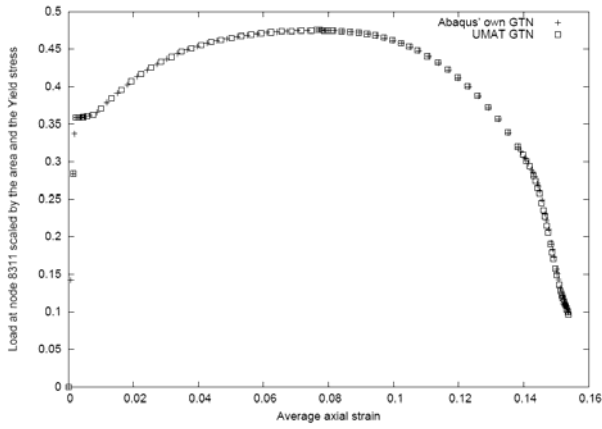


Fig. 11.  $\text{force}/(\pi r_w^2 \sigma_{PL})$  versus  $u_2^{8311}/l_w$

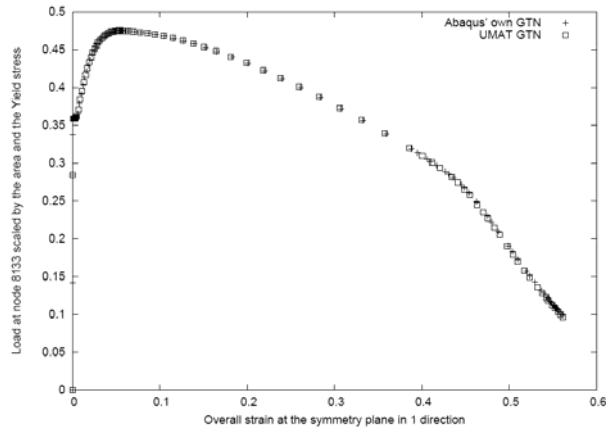


Fig. 12.  $\text{force}/(\pi r_w^2 \sigma_{PL})$  versus  $u_2^{1135}/r_a$

Good agreement was obtained with the ABAQUS porous plasticity model.

Element 1111 represents the mid-centre of the bar, where the voids would be expected to grow fastest and where fracture would ultimately occur. Figure 13 and 14 show the hydrostatic stress and void volume fraction respectively in element 1111 as a function of volumetric strain. The hydrostatic stress increased to a peak value and then decreased again. The void volume fraction increased continuously. Good agreement was obtained with the ABAQUS porous plasticity model, except for a small discrepancy at about  $\epsilon_{ii} = 1.1$  in each figure.

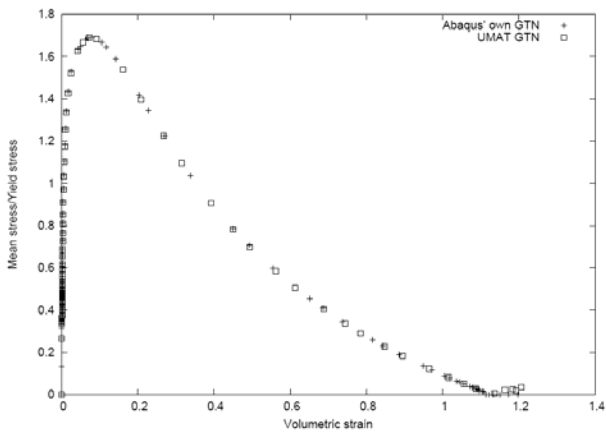


Fig. 13. Plot of  $\sigma_m/\sigma_{PL}$  versus volumetric strain  $\epsilon_{ii}$

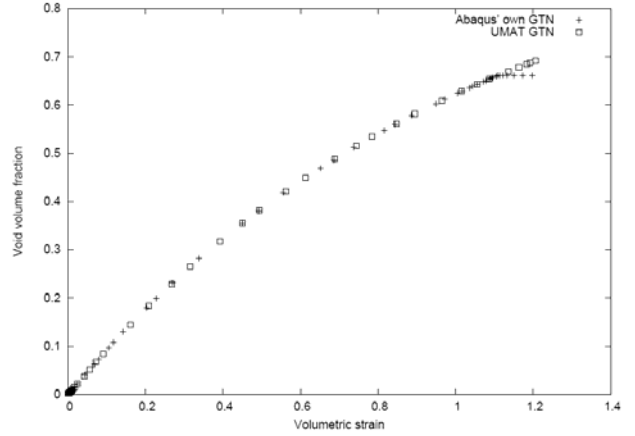


Fig. 14. Plot of void volume fraction versus volumetric strain  $\epsilon_{ii}$

Figure 15 shows a contour plot of the void volume fraction at an average axial strain of  $\epsilon_{22} = u_2^{8311}/l_w = 6 \times 10^{-3}$ . The result obtained using the ABAQUS porous plasticity model is shown on the left. The GTN model result is shown on the right. The small differences are due to different increments being matched to the average strain value in each case. It can be seen that the model correctly predicts the concentration of voids at the centre of the bar.

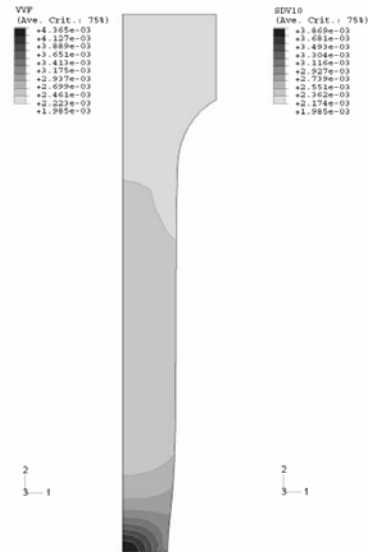


Fig. 15. Contour plots of void volume fraction

## CONCLUSIONS

The constitutive equations for the Gurson-Tvergaard-Needleman model for ductile damage have been presented in this paper, along with a description of a suitable trust region algorithm that can be used to solve the equations. This solution method has proved to be robust and efficient.

The model has been implemented as a Fortran 90 user material subroutine for use with ABAQUS/Standard. The subroutine allows the user to modify the yield surface to account for increased softening at large values of void volume fraction, due to void coalescence.

Example calculations are provided showing the results of applying the model to an axisymmetric bar. The analysis assumed no void coalescence and the results were comparable with those obtained using the porous plasticity model in ABAQUS/Standard.

## REFERENCES

1. A L Gurson, "Continuum theory of ductile rupture by void nucleation and growth: part 1 – yield criteria and flow rules for porous ductile materials", *J. Eng. Matl. Tech.*, **99**, 2-15, 1977.
2. V Tvergaard, "Influence of voids on shear band instabilities under plane strain conditions", *Int. J. Fract. Mech.*, **17**, 389-407, 1981.
3. V Tvergaard, "On localisation in ductile materials containing spherical voids", *Int. J. Fract.*, **18**, 237-252, 1982.
4. J Koplik and A Needleman, "Void growth and coalescence in porous plastic solids", *Int. J. Sol. Struct.*, **24**, No. 8, 835-853, 1988.
5. L Xia, C F Shih, "Ductile crack growth – I. A numerical study using computational cells with microstructurally-based length scales", *J. Mech. Phys. Solids*, **42**, 233-259, 1995.
6. C Ruggieri, T L Panontin, R H Dodds, "Numerical modelling of ductile crack growth in 3-D computational cell elements", *Int. J Fract.*, **82**, 95-97, 1998.
7. A S Gullerud, X Gao, R H Dodds, R Haj-Ali, "Simulation of ductile crack growth using computational cells: numerical aspects", *Engng. Fract. Mech.*, **66**, 65-92, 2000.
8. J Kim, X Gao, T S Srivatsan, "Modelling of void growth in ductile solids: effects of stress triaxiality and initial porosity", *Engng. Fract. Mech.*, **71**, 379-400, 2004.
9. J R Rice and D M Tracey, "On the ductile enlargement of voids in triaxial stress fields", *J. Mech. Phys. Solids*, **17**, 201, 1969.
10. V Tvergaard and A Needleman, "Analysis of cup-cone fracture in a round tensile bar", *Acta Metall.*, **32**, 157, 1984.
11. J Chakrabarty, "Theory of Plasticity", McGraw-Hill, 1987.
12. N Aravas, "On the numerical integration of a class of pressure-dependent plasticity models", *Int. J. Num. Methods. Eng.*, **24**, 1395-1416, 1987.

## ACKNOWLEDGEMENTS

This paper is published by permission of Serco Assurance. The authors would like to thank Prof. Andrew Sherry of The University of Manchester and Dr Martin Goldthorpe of Goldthorpe Associates for the analysis of the axisymmetric bar.

## APPENDIX – LINEARISATION MODULI

The linearisation are required for implementation of the backward Euler method in the Finite Element solver. They are provided in this Appendix without proof. The equations can be obtained by considering variations of stress and strain increments in Eqs. (1) and (6).

The linearisation moduli tensor  $D_{ijkl}$  is calculated using:

$$D_{ijkl} = \left( E_{ijkl}^{-1} + M_{ijkl} \right)^{-1} \quad (34)$$

where  $E_{ijkl}$  is the elasticity tensor, Eq. (9), and  $M_{ijkl}$  is the tensor:

$$M_{ijkl} = \left( M_{11} \delta_{mn} + M_{12} n_{mn} \right) \delta_{kl} + \left( M_{21} \delta_{mn} + M_{22} n_{mn} \right) n_{kl} + \frac{\Delta \varepsilon_{eq}^p}{\sigma_{eq}} \left( \frac{3}{2} \delta_{ik} \delta_{jl} - \frac{1}{2} \delta_{ij} \delta_{kl} - n_{ij} n_{kl} \right) \quad (35)$$

with

$$M_{ij} = \frac{A_{3-i,3-i} B_{ij} - A_{i,3-i} B_{3-i,j}}{A_{11} A_{22} - A_{12} A_{21}} \quad (36)$$

The coefficients  $A_{ij}$  and  $B_{ij}$  are calculated using:

$$\begin{aligned} A_{11} &= 3 \frac{\partial g}{\partial \sigma_{eq}} + \left( 3 \Delta \varepsilon_m^p \frac{\partial^2 g}{\partial \sigma_{eq} \partial H_\alpha} - \Delta \varepsilon_{eq}^p \frac{\partial^2 g}{\partial \sigma_m \partial H_\alpha} \right) c_{\alpha\beta}^{-1} \frac{\partial h_\beta}{\partial \Delta \varepsilon_m^p} \\ A_{12} &= - \frac{\partial g}{\partial \sigma_m} + \left( 3 \Delta \varepsilon_m^p \frac{\partial^2 g}{\partial \sigma_{eq} \partial H_\alpha} - \Delta \varepsilon_{eq}^p \frac{\partial^2 g}{\partial \sigma_m \partial H_\alpha} \right) c_{\alpha\beta}^{-1} \frac{\partial h_\beta}{\partial \Delta \varepsilon_{eq}^p} \\ A_{21} &= \frac{\partial g}{\partial H_\alpha} c_{\alpha\beta}^{-1} \frac{\partial h_\beta}{\partial \Delta \varepsilon_m^p} \\ A_{22} &= \frac{\partial g}{\partial H_\alpha} c_{\alpha\beta}^{-1} \frac{\partial h_\beta}{\partial \Delta \varepsilon_{eq}^p} \\ B_{11} &= - \Delta \varepsilon_m^p \left( \frac{\partial^2 g}{\partial \sigma_{eq} \partial \sigma_m} + \frac{\partial^2 g}{\partial \sigma_{eq} \partial H_\alpha} c_{\alpha\beta}^{-1} \frac{\partial h_\beta}{\partial \sigma_m} \right) + \\ &\quad \frac{1}{3} \Delta \varepsilon_{eq}^p \left( \frac{\partial^2 g}{\partial \sigma_m^2} + \frac{\partial^2 g}{\partial \sigma_m \partial H_\alpha} c_{\alpha\beta}^{-1} \frac{\partial h_\beta}{\partial \sigma_m} \right) \\ B_{12} &= - 3 \Delta \varepsilon_m^p \left( \frac{\partial^2 g}{\sigma_{eq}^2} + \frac{\partial^2 g}{\partial \sigma_{eq} \partial H_\alpha} c_{\alpha\beta}^{-1} \frac{\partial h_\beta}{\partial \sigma_{eq}} \right) + \\ &\quad \Delta \varepsilon_{eq}^p \left( \frac{\partial^2 g}{\partial \sigma_m \partial \sigma_{eq}} + \frac{\partial^2 g}{\partial \sigma_m \partial H_\alpha} c_{\alpha\beta}^{-1} \frac{\partial h_\beta}{\partial \sigma_{eq}} \right) \\ B_{21} &= - \frac{1}{3} \left( \frac{\partial g}{\partial \sigma_m} + \frac{\partial g}{\partial H_\alpha} c_{\alpha\beta}^{-1} \frac{\partial h_\beta}{\partial \sigma_m} \right) \\ B_{22} &= - \frac{1}{3} \left( \frac{\partial g}{\partial \sigma_{eq}} + \frac{\partial g}{\partial H_\alpha} c_{\alpha\beta}^{-1} \frac{\partial h_\beta}{\partial \sigma_{eq}} \right) \end{aligned} \quad (37)$$

In Eqs. (37),  $H_1 = \Delta \varepsilon_{eqM}^p$ ,  $H_2 = \Delta f$ ,  $h_1$  is the function on the right-hand side of Eq. (17), and  $h_2$  is the function on the right-hand side of Eq. (21). The tensor  $c_{\alpha\beta} = \delta_{\alpha\beta} - \frac{\partial h_\alpha}{\partial H_\beta}$ .